Aerosol Science and Technology
Publication details, including instructions for authors and subscription information:
http://www.tandfonline.com/loi/uast20

Deposition of Fiber in the Human Nasal Airway

Wei-Chung Su [a] & Yung Sung Cheng [a]
[a] Lovelace Respiratory Research Institute , Albuquerque, New Mexico, USA
Published online: 23 Feb 2007.

To cite this article: Wei-Chung Su & Yung Sung Cheng (2005) Deposition of Fiber in the Human Nasal Airway, Aerosol Science and Technology, 39:9, 888-901

To link to this article: http://dx.doi.org/10.1080/02786820500295685

Aerosol Science and Technology, 39:888–901, 2005

ISSN: 0278-6826 print / 1521-7388 online
DOI: 10.1080/02786820500295685

Deposition of Fiber in the Human Nasal Airway

Wei-Chung Su and Yung Sung Cheng
Lovelace Respiratory Research Institute, Albuquerque, New Mexico, USA

Inhalation is the main route for aerosol entering the human body. Many occupational lung diseases are associated with exposure to fiber aerosol in the workplace. However, very few studies to date have been conducted for investigating fiber deposition in the human airway. As a result, there is a notable lack of information on the nature of the fiber deposition pattern in the human respiratory tract. With this in mind, this research consisted of a large number of experimental works to investigate the effects of fiber dimension on the deposition pattern for a human nasal airway. Carbon fibers with uniform diameter (3.66 μm) and polydispersed length were adopted as the test material. Deposition studies were conducted by delivering aerosolized carbon fibers into a nasal airway replica (encompassing the nasal airway regions from vestibule to nasopharynx) at constant inspiratory flow rates of 7.5, 15, 30, and 43.5 l/min. Fibers deposited in each nasal airway region were washed out and the length distribution was determined by microscopic measurement. The results showed that impaction is the dominant deposition mechanism. Most of the fibers with high inertia deposited in the anterior region of the nasal airway (vestibule and nasal valve). In contrast, fibers with low inertia were found to pass through the entire nasal airway easily and collected on the filter at the outlet. Comparing the deposition results between fibers and spherical particles, our data showed that the deposition efficiencies of fibers are significantly lower than that of spherical particles, which implies that the inhaled fibers could pass through the entire nasal airway comparatively easier than spherical particles. Thus, relatively more fibers would be able to enter the lower respiratory tract.

INTRODUCTION

Aerosol deposition in the human airway has attracted considerable attention due to its importance in occupational health. The health effects of exposure to aerosol depend on the region of the airway on which the particles (including fibers) deposit. Numerous studies have documented aerosol deposition in human airway replicas for spherical particles in inertia regime (Swift 1991; Cheng et al. 1999, 2001a, 2001b; Zwartz and Guilmette 2001; Kelly et al. 2004; Zhou and Cheng, 2005). From those studies, deposition efficiencies were reported for certain regions of the human airway, and theoretical equations have also been proposed. Both experimental and theoretical data were found to be in good agreement. However, for fiber particles, the situation was less satisfactory. Although it is believed that the deposition pattern of fibers might be different from that of spherical particles (WHO 2000), very limited studies to date have been conducted for fiber deposition in the human airway replica (Sussman et al. 1991). Only few experimental data are available for fiber deposition in a bifurcating tube (Myojo 1987, 1990).

Fibers are elongated particles with a length more than 5 μm and an aspect ratio, β (the ratio of the length to the diameter), over 3 (NIOSH 1994). The aerodynamic diameter of a fiber depends primarily on its diameter and only slightly on its length (Stöber et al. 1970; Cheng et al. 1995). There are four mechanisms involved in fibers depositing in a human airway: sedimentation, impaction, diffusion, and interception. Each deposition mechanism is significant in a certain fiber dimension range and insignificant in others. It has been reported that fiber dimensions and biopersistence play an essential role on the pathogenesis of fiber-related lung diseases (Timbrell 1982; Lippmann 1990; Hill et al. 1995; Bernstein et al. 2001) such as long and thin fibers have greater toxicity than short and thick fibers. Many occupational diseases were found to be associated with the deposition of aerosolized fibers in certain regions of the human airway. For example, the deposition of asbestos in human lung increases the incidence of lung cancer, mesothelioma, and fibrosis (Selikoff and Lee 1978; IARC 1987).

In recent years, occupational exposure to asbestos fibers has decreased because this material was replaced (due to its toxicity) in many applications with man-made vitreous fibers (MMVFs), including glass, ceramic, and silicon fibers. Nevertheless, research conducted in laboratory animals has shown that some MMVFs may have biological effects similar to those of asbestos (Miller et al. 1999; Hesterberg and Hart 2001; IARC 2002; Kamstrup et al. 2002). Therefore, new information is needed to provide more information on the deposition of MMVFs in the human airway. Because there is no reliable instrument available for detecting fiber size and number, and also because

Received 13 May 2005; accepted 8 August 2005.
The authors are grateful to W. T. Fan for technical assistance, and V. Fisher for reviewing this manuscript. This project is sponsored by NIOSH grant R01 OH003900.
Address correspondence to Wei-Chung Su, Lovelace Respiratory Research Institute, 2425 Ridgecrest Drive, SE, Albuquerque, New Mexico 87108, USA. E-mail: wsu@LRRI.org

of the difficulty and time-consuming effort required for the post-experimental process for a replica deposition experiment (sample preparation and fiber measurement), it is extremely hard and complicated to conduct a fiber deposition study in laboratory. Moreover, the ethical constraints severely limit the use of fibers in a human volunteer. As a result, there is a notable lack of experimental data for fiber deposition in the human airway presently. The lack of experimental data not only hampers the verification of the available lung deposition model, but the nature of human airway fiber deposition also remains unknown.

This research attempts to fill this gap above by obtaining sufficient experimental data of fiber deposition in a human airway to investigate the association among fiber characteristics, the deposition mechanism, and the deposition pattern. In this study, a human nasal airway was chosen because the nasal airway is the major entry to the human respiratory tract, and acts as a first line of defense and also as a filtration system in preventing hazardous aerosols from entering the lung. The deposited fraction of the inhaled fiber acquired from the nasal airway could directly indicate that the remaining fraction of the inhaled fiber entered the lower respiratory tract. The nasal airway replica used in this research has realistic and well-defined airway geometry, and has been used for several particle deposition studies. In addition, a MMVF-like fiber—carbon fiber with uniform diameter and different lengths—was used as the test material. Using a monodisperse-diameter fiber is a new approach in deposition studies since it provides a simple way to obtain fiber dimension (length measurement only) and a sure way to determine the effect of fiber length on the deposition pattern. Because fiber deposition in the human airway is believed to be a function of its physical characteristics, for occupational health purposes, the information obtained from this research is useful in assessing the exposure dosimetry of fiber and predicting fiber deposition for other types of fibers, including asbestos and new MMVFs being developed.

EXPERIMENTAL METHOD

Nasal Airway Replica

A human nasal replica of a nonsmoking Caucasian male (53 years of age, 73 kg in body mass, and 173-cm tall) was made based on in vivo magnetic resonance imaging (MRI), with an image taken every 3 mm (Guilmette and Gagliano 1994). The original images obtained from these MRIs were digitized with a GRAF/PEN sonic digitizer (SAC, Southport, Connecticut). Based on these digital data, three-dimensional surfaces were constructed for adjacent perimeter traces with a computer-assisted design software (SmartCAM, Point Control Co., Eugene, Oregon). The physical nasal replica was made by using 1.5-mm-thick acrylic plates and milling with a computer-controlled micro-milling machine (CAMM 3, Roland DG, Los Angeles, California). The entire nasal replica contains 77 acrylic plates (115.5 mm total length) and consists of complete nasal airway structures, including anterior region (first 25 plates: 0–37.5 mm, with vestibule and nasal valve subregions), turbinate region (middle 32 plates: 37.5–85.5 mm, with front and rear turbinate subregions), and posterior (nasopharynx) region (last 20 plates: 85.5–115.5 mm). The turbinate region was subdivided into superior turbinate (ST) and also known as the olfactory area, middle turbinate (MT), and inferior turbinate (IT) sections. Figure 1 shows the structure and sections of the nasal airway replica. Prior to the deposition experiment, silicon oil (550 Fluid, Dow Corning Co., Midland, Michigan) was applied to the inside surface of the replica to simulate the condition of the moist wall in a real human nasal airway. The oil coating not only helps fibers stick to the region where they are deposited, but it also smooths and seals the nasal airway. The nasal cast was leak-tested and charge-tested prior to each deposition experiment. Many researchers have used this replica in our laboratory for particle deposition studies (Guilmette et al. 1994; Cheng et al. 2001b; Zwartz and Guilmette 2001) and the results have shown that this replica provides reliable information for particle deposition in a human nasal airway.

Test Fiber Material

Test carbon fibers were provided by Hercules, Inc. (Wilmington, Delaware). These carbon fibers are black in color, conductive, monodisperse in diameter (3.66 μm), polydisperse in length, and density measured at 1.83 g/cm^3. The fiber shape, diameter distribution, and length distribution are shown in Figure 2 (the statistical data were obtained after fibers passed through the generation process). This carbon fiber has been used for a size classification study in our laboratory (Chen et al. 1993). The test fiber material contains cylindrical fibers and fiber debris. Preliminary investigation showed that the fiber debris is mainly in the 1–5 μm size range and has a number concentration of 27% of the total fiber. In this research, fibers with an aspect ratio of greater than 3:1 were counted as contributing to the deposition data. However, fibers with lengths shorter than 10 μm were discarded and were not recorded.

The aerodynamic diameter (d_{ae}) of a carbon fiber could be approximately calculated by the equations below (Stöber 1972):

$$d_{ae} = d_{ve}\sqrt{\rho/\rho_o\kappa} \qquad [1]$$

where d_{ve} is the volume equivalent diameter, ρ is the density of carbon fiber, ρ_o is the density of water, and κ is the dynamic shape factor for a prolate spheroid. For a prolate spheroid flying in the air with its long axis orientating perpendicular to the flow direction, the dynamic shape factor is $\kappa_\perp$

$$\kappa_\perp = \frac{\frac{8}{3}(\beta^2-1)\beta^{-1/3}}{\frac{2\beta^2-3}{\sqrt{\beta^2-1}}\ln(\beta+\sqrt{\beta^2-1})+\beta} \qquad [2]$$

where β is the aspect ratio. The dynamic shape factor is $\kappa_\parallel$, if the long axis of a prolate spheroid orientates parallel to the

(a)

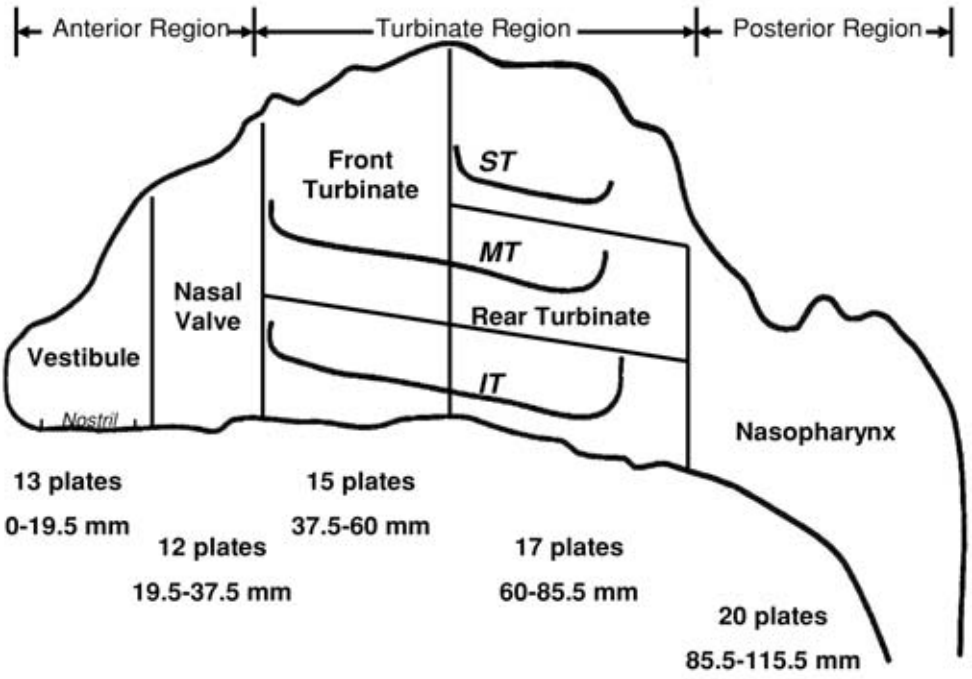

(b)

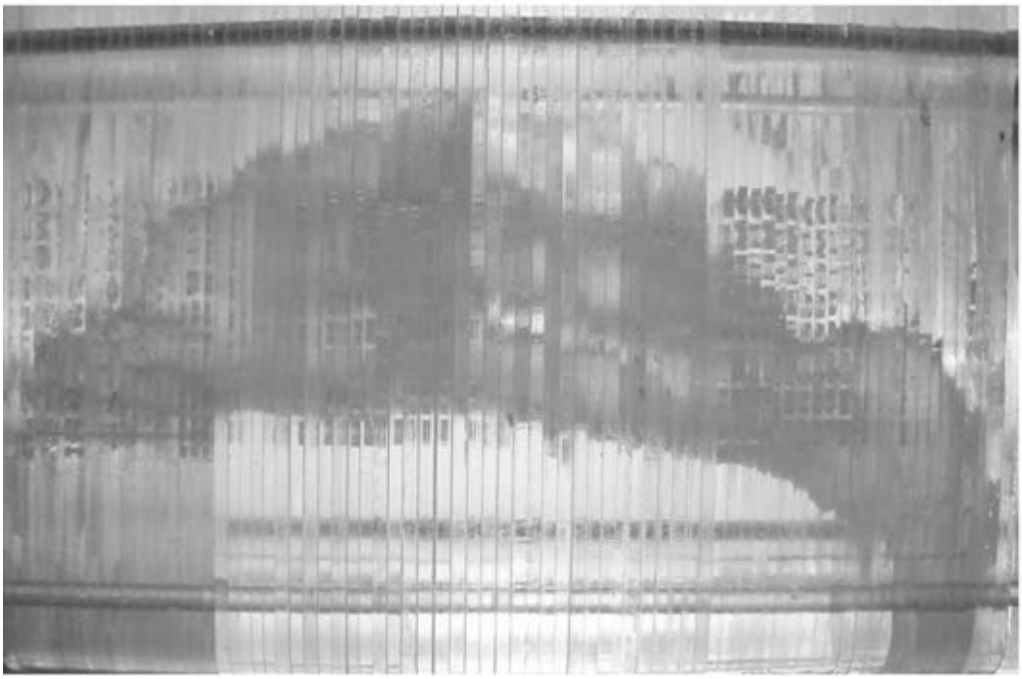

FIG. 1. Structure and regions of the human nasal airway replica (a) schematic diagram, (b) physical model.

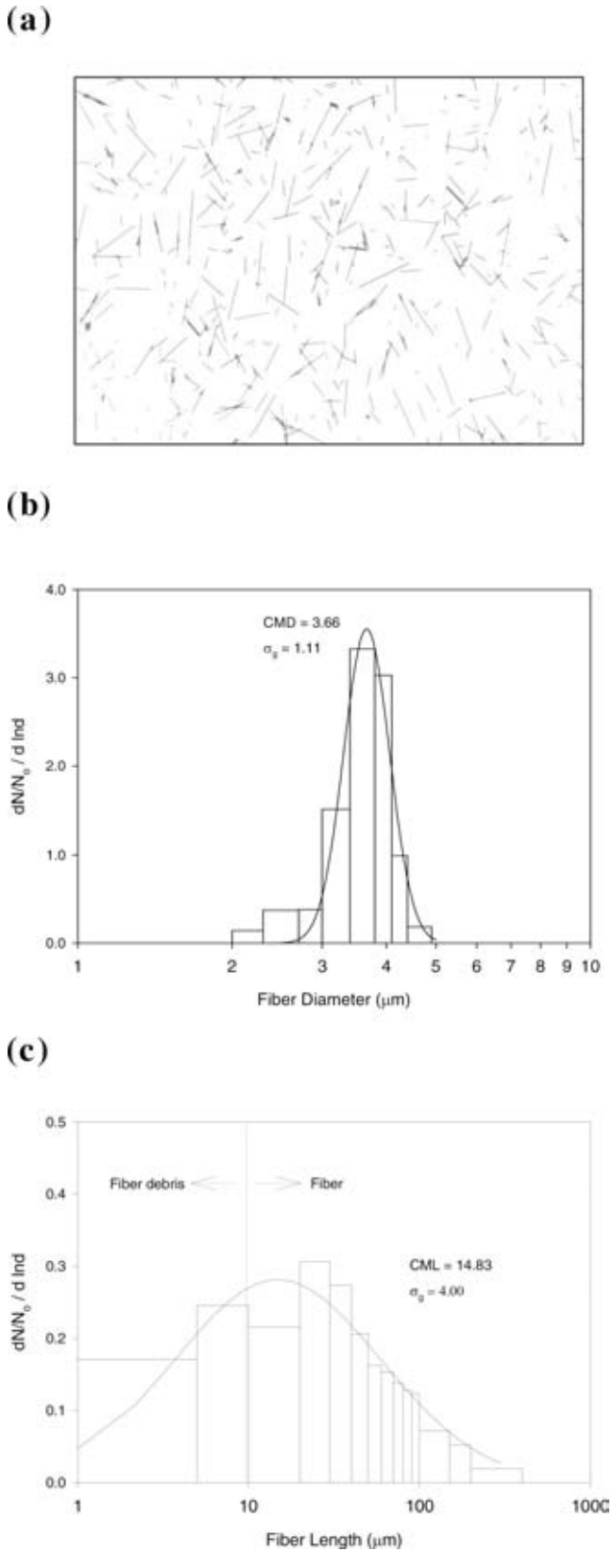

FIG. 2. Characteristics of carbon fibers: (a) microscopic view, (b) diameter, and (c) length distribution.

flow direction.

$$\kappa_{\parallel} = \frac{\frac{4}{3}(\beta^2-1)\beta^{-1/3}}{\frac{2\beta^2-1}{\sqrt{\beta^2-1}}\ln(\beta+\sqrt{\beta^2-1})-\beta} \quad [3]$$

Finally, if the orientation of a prolate spheroid is randomly in the air, the dynamic shape factor is κ_r and can be written as (Happel and Brenner 1973)

$$\frac{1}{\kappa_r} = \frac{1}{3\kappa_{\parallel}} + \frac{2}{3\kappa_{\perp}} \quad [4]$$

Based on the equations above, for a 20-μm-long carbon fiber in the airflow (diameter = 3.66 μm) with its long axis orientating perpendicular to the flow direction (dynamic shape factor = $\kappa_{\perp}$), the aerodynamic diameter of the fiber, $d_{ae(\perp)}$, is 8.4 μm. On the other hand, if the fiber's long axis is parallel to the flow direction (dynamic shape factor = $\kappa_{\parallel}$), the aerodynamic diameter, $d_{ae(\parallel)}$, is 9.7 μm. However, if the fiber orientates randomly in the air (dynamic shape factor = κ_r), the aerodynamic diameter, $d_{ae(r)}$, is 8.8 μm. In contrast, for a 100-μm-long carbon fiber in the air, its $d_{ae(\perp)}$, $d_{ae(\parallel)}$, and $d_{ae(r)}$ are 10.4 μm, 13.0 μm, and 11.3 μm, respectively.

Experimental Setup and Procedure

Figure 3 shows the experimental setup for the fiber deposition study. The experimental apparatus included a fiber generator, a charge neutralizer, the human airway replica, and a filter unit. The fiber aerosol was generated by a small-scale powder disperser (SSPD, Model 3433, TSI Inc., St. Paul, Minnesota). Dispersed fibers were first delivered to the Kr^{85} charge neutralizer. Fibers passing through the neutralizer were at Boltzmann equilibrium and then delivered to the nasal replica. Fibers impacting the nasal airway were captured and remained in place due to the silicon oil coating. A 47-mm filter unit was attached to the nasopharynx, the location of exit, for collecting fibers that passed through the replica. In our study, four constant inspiratory flow rates (7.5, 15, 30, and 43.5 l/min) were used to cover the range of adult breathing under different activities. Three experiments were conducted for each flow rate to determine the average deposition values. A typical experiment lasted 5–20 minutes, depending on the inspiratory flow rate (43.5–7.5 l/min), and the SSPD was set to a rotation plate speed of 2, all of which have been proved to allow a sufficient number of fibers to deposit in the replica.

Sample Preparation

After the experiments, the nasal airway replica was divided into regions/subregions based on the nasal airway structure. Every single plate was carefully disassembled from the airway replica and washed by brushing in filtered isopropyl alcohol. Plates from the turbinate region were subdivided into ST, MT, and IT sections and washed individually. Fibers washed out from

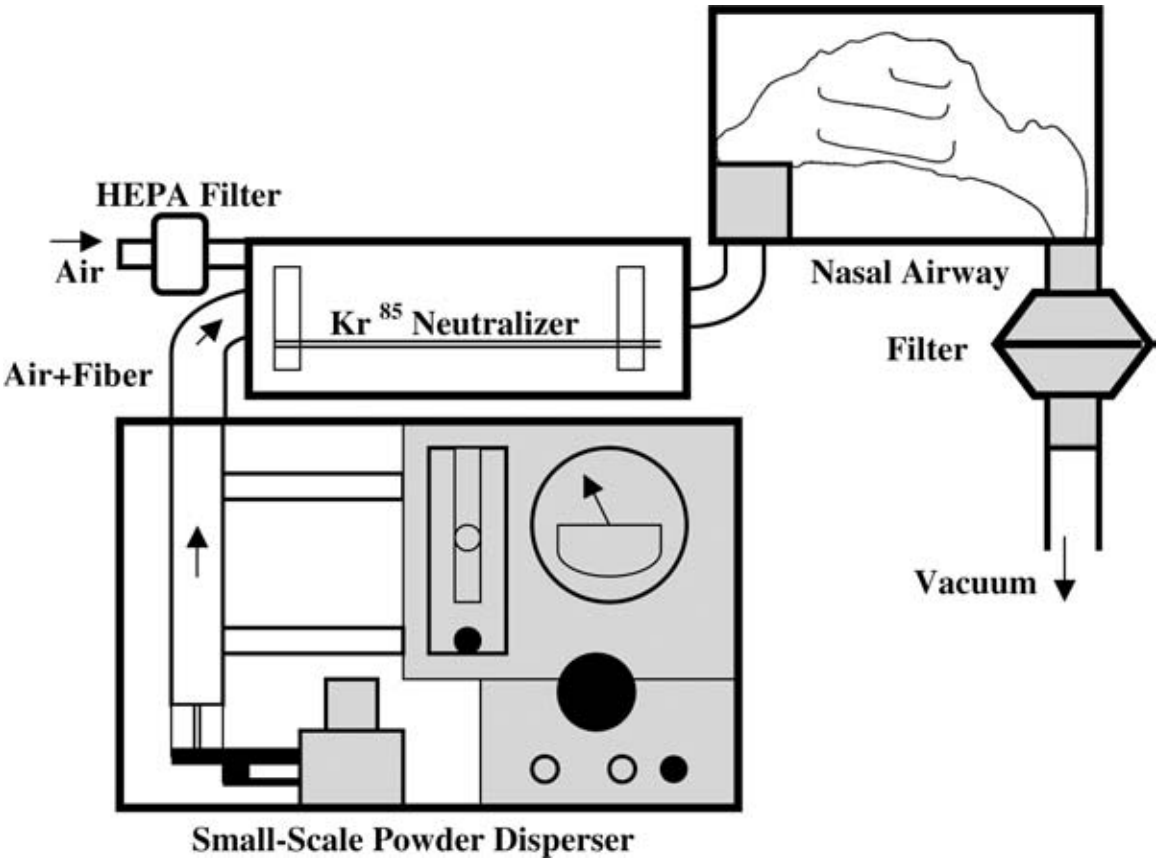

FIG. 3. Schematic diagram of the experimental setup for the fiber deposition study.

the plates were continually agitated so that they were well mixed in the alcohol solution. The 47-mm filter at the outlet was treated with the same process to remove collected fibers to the alcohol solution. All solutions were then vacuum-filtered by a 25-mm filtration assembly to allow fibers to uniformly deposit on a 25-mm mixed cellulose ester membrane filter (GSWP, Millipore Co., Bedford, MA). The filters were then dried at room temperature in a dust-free environment and prepared as the sample slide for later microscopic counting/measurement. In total, nine sample slides were acquired for each run of the deposition experiment, and each slide represented one region/subregion of the nasal airway.

Fiber Counting and Length Measurement

The fiber sample slides were examined by an optical microscope (BH-2, Olympus Optical Co., Tokyo, Japan) with G22 Walton-Beckett graticule (Pyser-SGI Ltd., Kent, UK). The total number of fibers and the length of individual fibers in a viewing area were determined based on National Institute of Occupational Safety and Health (NIOSH) method 7400. Measured fiber lengths were recorded on a self-developed counting table. This counting table has 14 length categories starting at 10 μm with increasing intervals every 10 μm. In this way, the fiber length distribution, the total number of fibers, and the average number of fibers in one viewing area were obtained for each sample slide. Figure 4 shows an example of fibers in a viewing area (under 40$\times$ magnification) while conducting the counting/measurement procedure. In this study, each sample slide was counted/measured for 200 fibers or 200 viewing areas, depending on whichever came first.

RESULTS

Deposition Pattern

The fiber deposition pattern was acquired after the deposition information was obtained on all nasal airway regions and subregions. Figures 5–8 show the fiber deposition patterns for four inspiratory flow rates in combined length categories. The deposition fraction shown for a specific region or subregion is the average value from three experiments at that specific region or subregion. As shown in Figure 5, the deposition pattern for inspiratory flow rate of 7.5 l/min indicates that most of the fibers passed through the nasal airway and were collected on the filter. The fiber deposition fraction in each nasal airway subregion was typically below 10% for every length category. Only one subregion, the IT of the front turbinate, was slightly larger than 10% in the long fiber ($>$100 μm) category (Figure 5d).

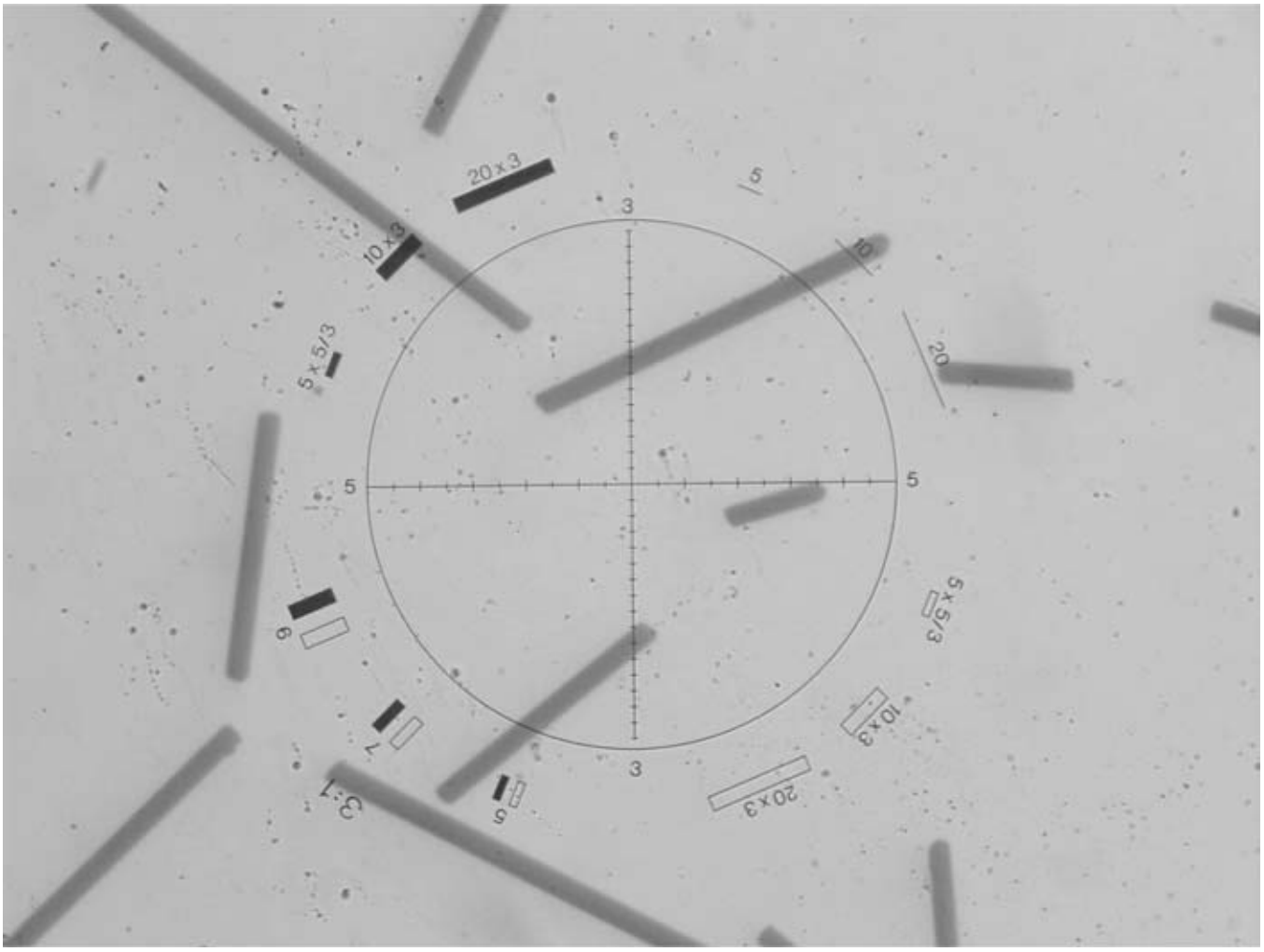

FIG. 4. Fiber counting/measuring with G22 Walton-Beckett gratitude (under 400× magnification).

In addition, the number of fibers collected on the filter decreases as the fiber length increases, which implies that the longer the fiber the harder it is for it to pass through the nasal airway.

Figure 6 shows the deposition pattern for a 15 l/min inspiratory flow rate. As can be seen, a considerable percentage of fibers were deposited in the nasal airway. Most of the fibers were in the anterior region (vestibule and nasal valve) and some in the MT of the front turbinate. However, there was still a considerable percentage of short fibers found passing through the entire nasal airway (33%; Figure 6a). Similarly, as shown in Figure 5, the percentage of fibers passing through the nasal airway in Figure 6 decreases as the fiber length increases. In the long fiber category (>100 μm; Figure 6d), only 11% of long fibers passed through the nasal airway and collected on the filter. In the turbinate region, very few fibers were found in the rear turbinate subregion and only a few fibers deposited in the front turbinate subregion, especially in the MT. Almost no fibers were deposited in the posterior region (nasopharynx).

As shown in Figure 7, for an inspiratory flow rate of 30 l/min, the majority of the fibers were deposited in the anterior region, especially in the vestibule. The deposition fractions in the anterior region were between 77% (short fibers) and 88% (long fibers). Compared with the deposition pattern of the 15 l/min inspiratory flow rate (Figure 6), the percentage of fibers collected on the filter in Figure 7 was significantly decreased, which indicates that the fibers had difficulty passing through the entire nasal airway, whether or not they are short or long fibers. On the other hand, similar to the result of the 15 l/min inspiratory flow rate (Figure 7), very few fibers were found in the rear turbinate and nasopharynx regions.

The deposition pattern for a 43.5 l/min inspiratory flow rate is shown in Figure 8. As can be seen, the deposition patterns are similar to those for an inspiratory flow rate of 30 l/min (Figure 7), but relatively more long fibers (fibers $>$ 70 μm) were found in the nasal valve and front turbinate subregions. In Figure 8, fibers are mainly deposited in the vestibule, nasal valve, and the front turbinate subregions. More than 99% of the fibers were deposited

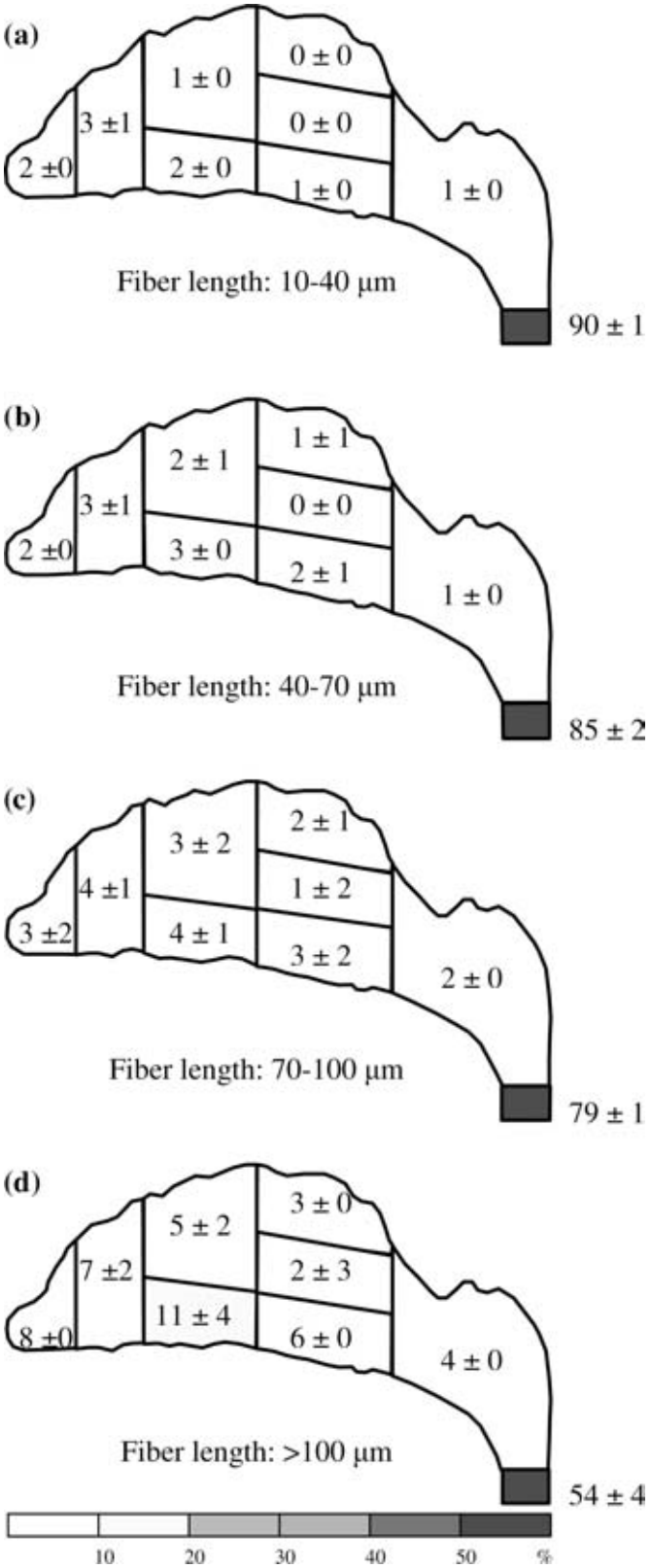

FIG. 5. Fiber deposition map for an inspiratory flow rate of 7.5 l/min. Deposition fractions for each region and subregion are shown in percent (0 represents the value of the fraction <0.5%).

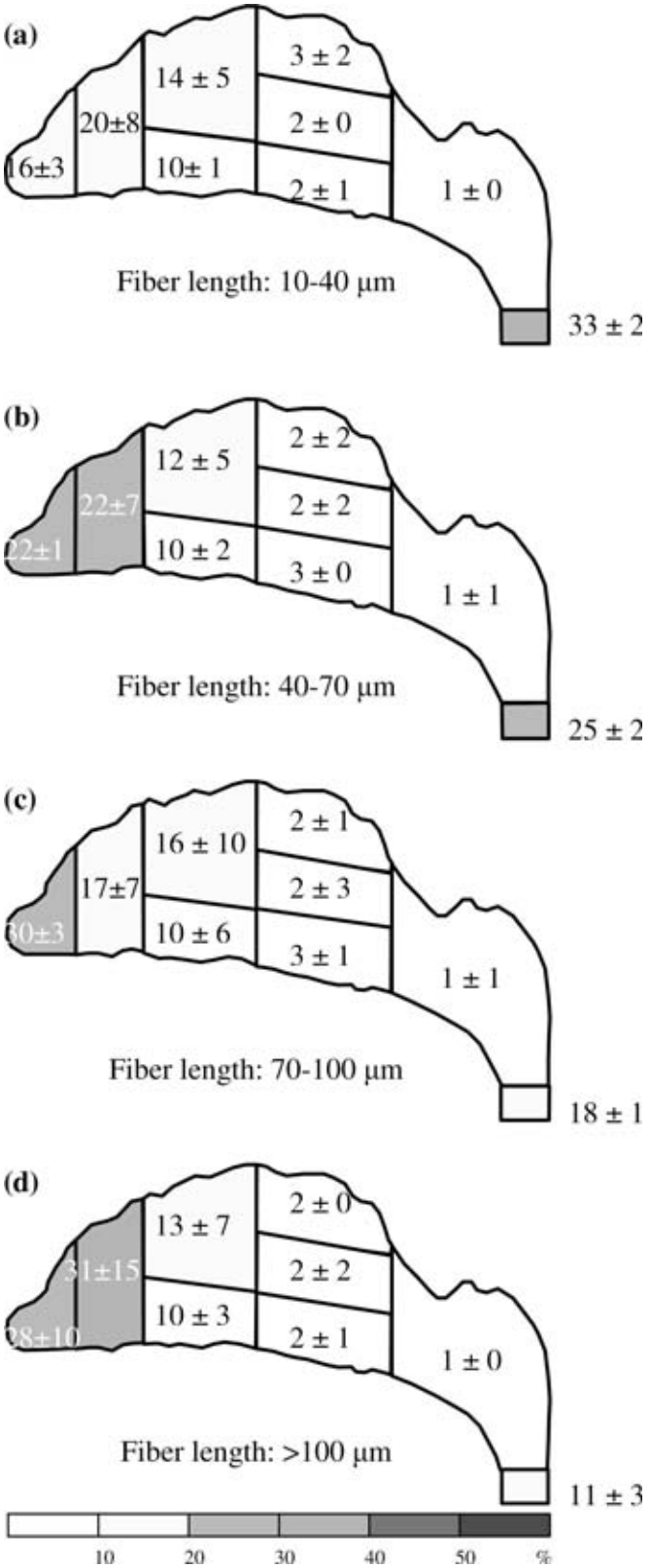

FIG. 6. Fiber deposition map for an inspiratory flow rate of 15 l/min. Deposition fractions for each region and subregion are shown in percent (0 represents the value of the fraction <0.5%).

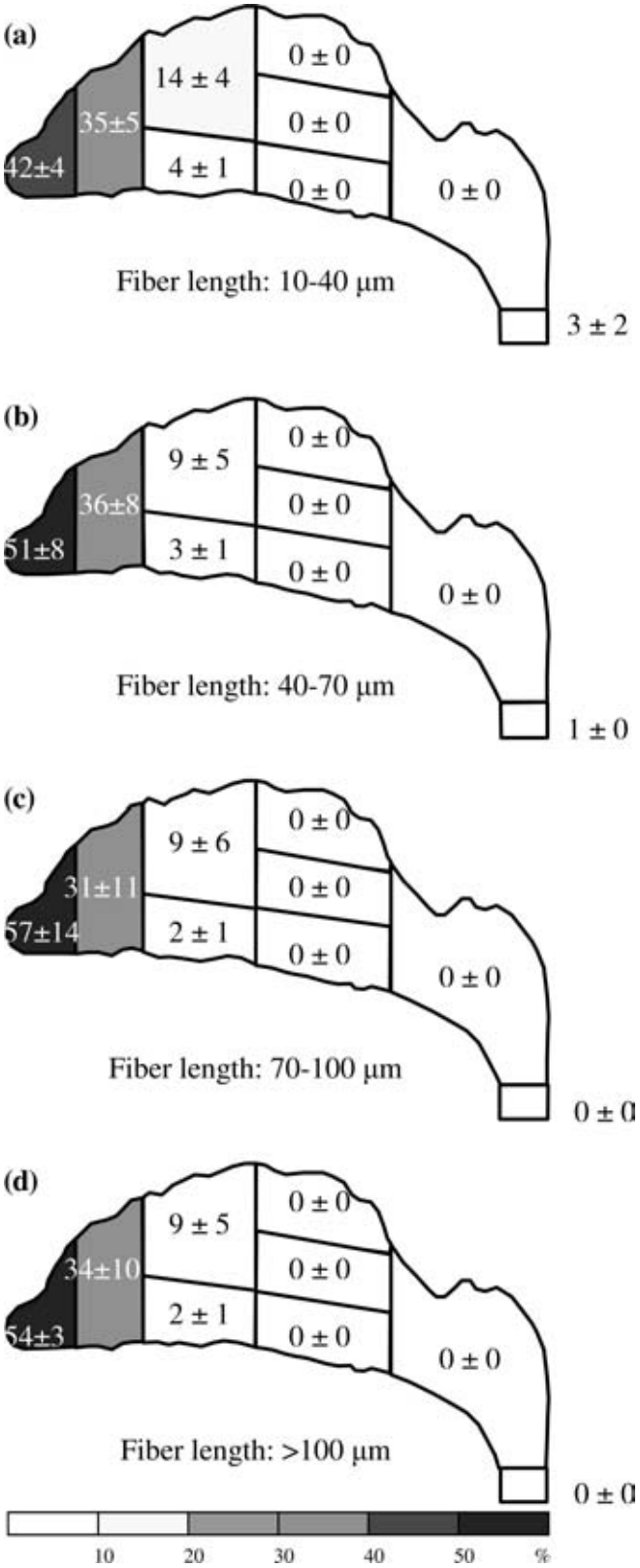

FIG. 7. Fiber deposition map for an inspiratory flow rate of 30 l/min. Deposition fractions for each region and subregion are shown in percent (0 represents the value of the fraction <0.5%).

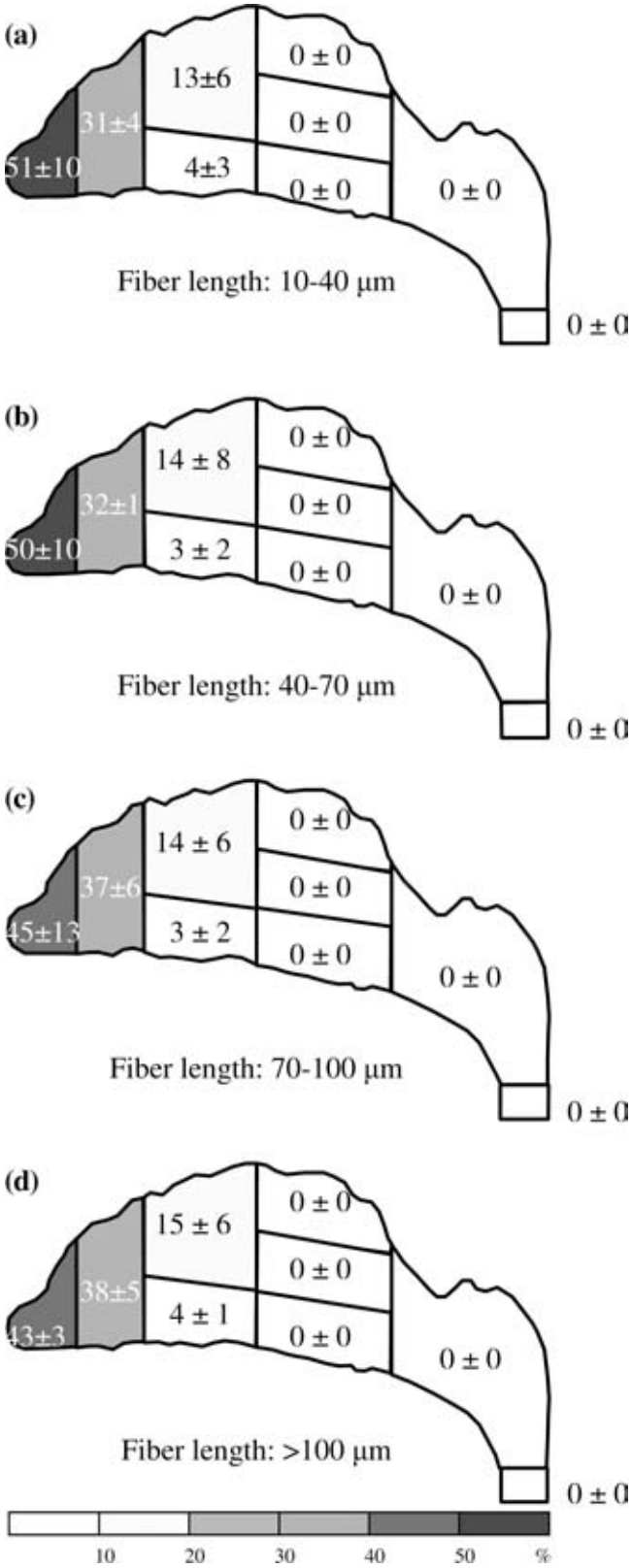

FIG. 8. Fiber deposition map for an inspiratory flow rate of 43.5 l/min. Deposition fractions for each region and subregion are shown in percent (0 represents the value of the fraction <0.5%).

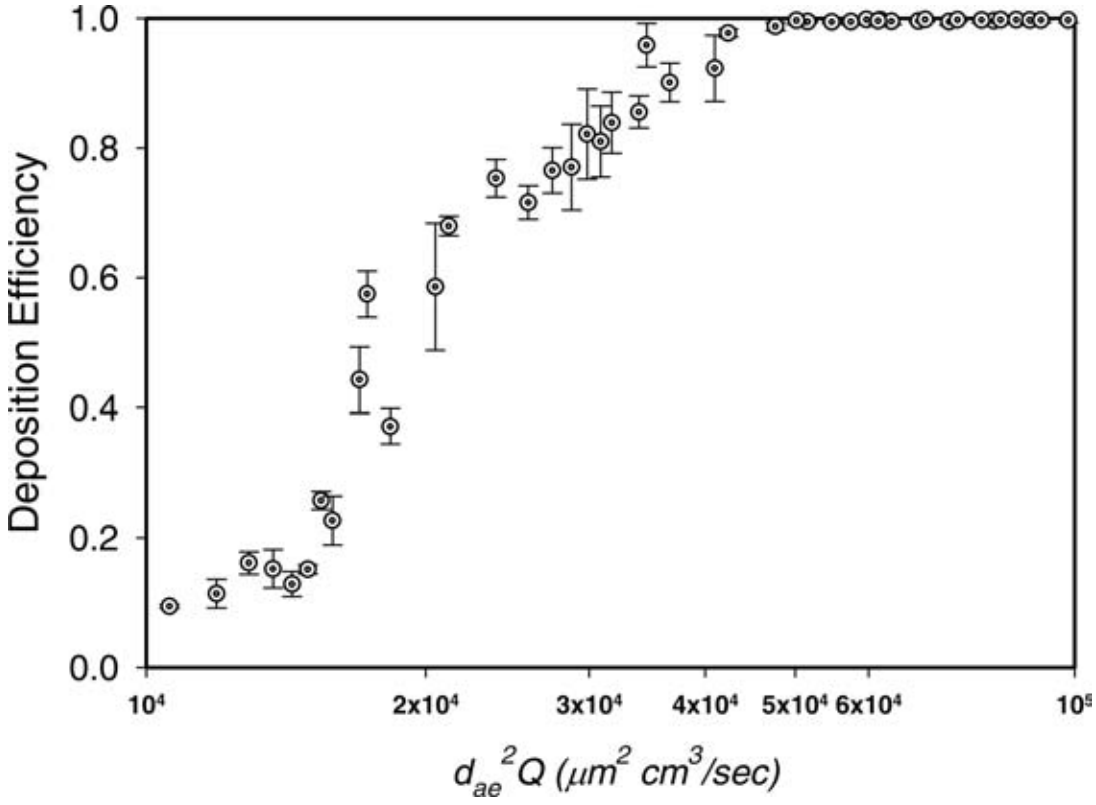

FIG. 9. The deposition efficiency as a function of impaction parameter for fiber deposition in the human nasal airway.

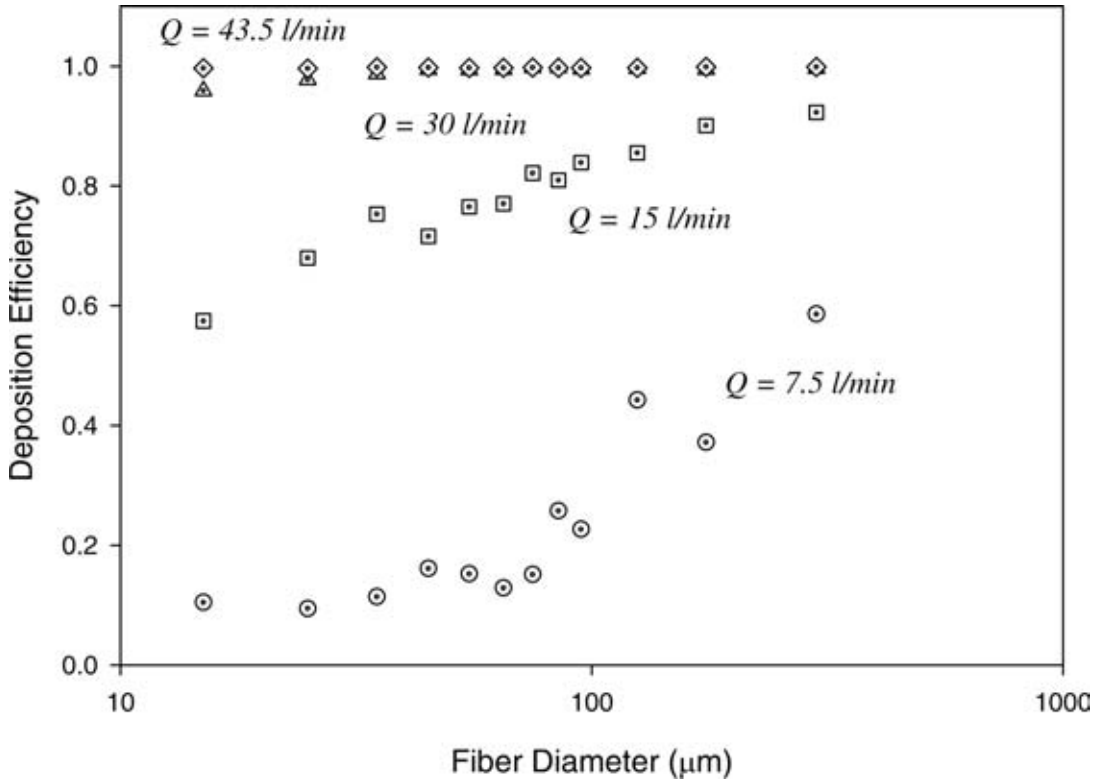

FIG. 10. Deposition efficiency as function of fiber length for fiber deposition in the human nasal airway using different inspiratory flow rates.

in these places for each fiber length category. Extremely few fibers (<0.5%) passed the nasal airway and collected on the filter.

Deposition Efficiency

Figure 9 shows the deposition efficiency as a function of impaction parameter (fiber inertia) for fiber deposition in a human nasal airway. The deposition efficiency, η, of the entire nasal airway for specific length category, i, was calculated by

$$\eta = N_{nasal(i)}/\left(N_{nasal(i)+}\ N_{filter(i)}\right) \quad [5]$$

where $N_{nasal(i)}$ is the number of fibers deposited in the nasal airway for length category i, and $N_{filter(i)}$ is the number of fibers, in the same length category i, collected on the filter. The fiber impaction parameter which represents the fiber inertia was calculated by

$$d_{ae}{}^2 Q \quad [6]$$

where d_{ae} is the aerodynamic diameter of fiber, and Q is the inspiratory flow rate. For $d_{ae}{}^2 Q$ throughout this article, d_{ae} is represented by $d_{ae(\mathrm{r})}$ since the actual orientation of fibers in the inhaled air flow is unknown. As seen in Figure 9, the deposition efficiency is positively related to the impaction parameter. The deposition efficiency increases as the impaction parameter increases. At the small and large values of the impaction parameter, the deposition efficiency increases slowly as the impaction parameter increases. However, the deposition efficiency rises rapidly and steeply at the impaction parameter range 1.5×10^4 to 3.5×10^4. Overall, the deposition efficiency is under 20% when the impaction parameter is smaller than 1.5×10^4, and the deposition efficiency closes to 99% when the impaction parameter reaches 5.0×10^4.

Figure 10 shows the deposition efficiency as a function of fiber length for different inspiratory flow rates. As shown in Figure 10, for a given inspiratory flow rate ranging from 7.5 to 30 l/min, the deposition efficiency rises steadily as the fiber length increases. On the other hand, for a given fiber length, the deposition efficiency increases significantly as the inspiratory flow rate increases. For short fibers smaller than 40 μm, their deposition efficiency increased approximately tenfold from 0.1 to 1.0 as the inspiratory flow rate increased from 7.5 to 43.5 l/min. For the same increase of the flow rate, long fibers which are larger than 100 μm at least double their deposition efficiency.

DISCUSSION

Deposition Mechanism of Carbon Fiber in the Nasal Airway

It has been shown in the previous section, for a high inspiratory flow rate of 30 l/min and up, the fiber deposition "hot spot" is at the anterior region. More than 77% of fibers were deposited there. For the median inspiratory flow rate of 15 l/min, the deposition pattern is similar. The anterior region is still the hot spot, but the deposition fraction is a bit smaller. However, for the low inspiratory flow rate (7.5 l/min), the anterior region is no longer the area where fibers are likely to deposit and most of the fibers passed through the entire nasal airway. These results imply that the deposition of the test fiber in the nasal airway (especially in the anterior region) is due to inertia. Moreover, as shown in Figure 9, the deposition efficiency for the entire nasal airway increases as the impaction parameter increases. It reconfirms that impaction is the dominant deposition mechanism in the present research, and this experimental result might occur because the carbon fibers used in our research are all in the high inertia regime.

When air is inhaled into the nostril, it experiences a sharp turn in the vestibule area. The airflow makes a nearly 90-degree turn from a vertical to a horizontal direction. Fibers having low inertia can follow the airstream closely and make the turn easily to avoid impaction on the bend area of the vestibule. Therefore, there were not many low-inertia fibers deposited around the vestibule (Figure 11a), and most of the low-inertia fibers passed beyond

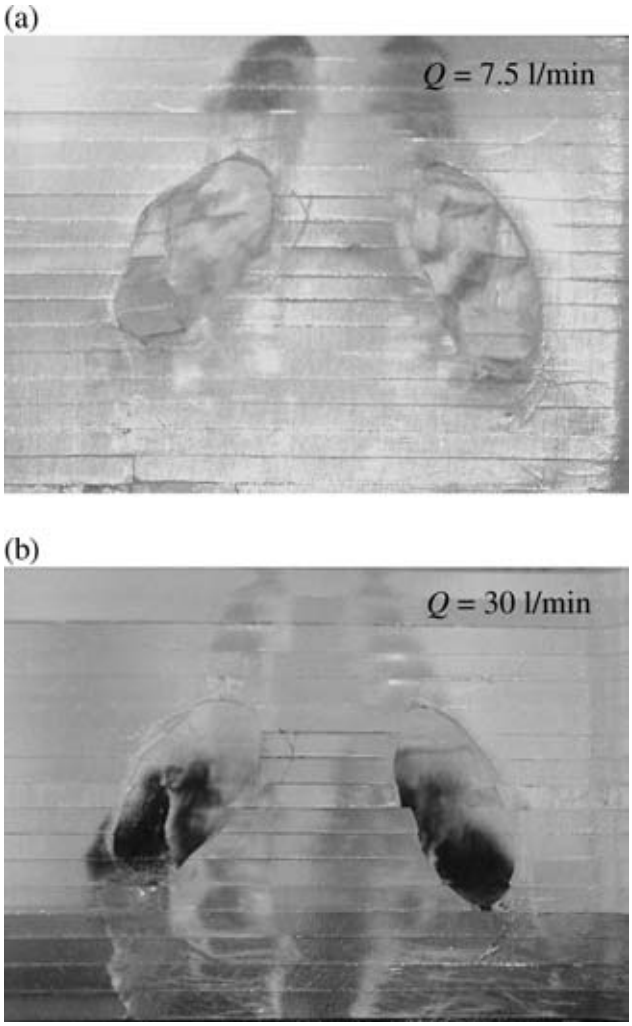

FIG. 11. Fiber deposition in the vestibule area for a inspiratory flow rate of (a) $Q = 7.5$ l/min, and (b) $Q = 30.0$ l/min (bottom view of the nostril entrance).

the anterior region and were delivered deeper in the nasal airway. On the other hand, fibers with high inertia have difficulty flowing easily with the airstream. As a result, they were not able to make turns with the airstream, and most of these high-inertia fibers impacted on the roof of the vestibule region as shown in Figure 11b. A similar result was also observed by Zwartz and Guilmette (2001) in the deposition study of spherical particles using the same nasal airway replica.

Long versus Short Fibers

Figure 12a and b show the comparison of deposition fractions in the anterior region (vestibule and nasal valve subregions) and in the filter for short fibers (fiber length = 10 to 20 μm; $d_{ae(r)} = 7.6$ to 8.8 μm) and long fibers (fiber length > 200 μm; $d_{ae(r)} > 12.3$ μm). As can be seen, the deposition trends of the anterior region and filter are similar for both fiber categories. Only the values of the deposition fraction are different for a specific flow rate. Generally, in a low inspiratory flow rate range, there are more fibers deposited on the filter than on the anterior region, which indicates that if the inhaled fibers have low inertia, they pass easily through the entire nasal airway and enter the larynx or even the trachea-bronchi and the deep lung. As the inspiratory flow rate increases, the deposition fraction in the anterior region starts to increase rapidly while there is a steep decrease in fibers passing through the nasal airway. In the high inspiratory flow rate range ($Q \geq 30$ l/min), there are a greater number of fibers deposited in the anterior region (>70%) than collected on the filter (<10%), which indicates that most of the fibers inhaled are impacted and remained in the nostril area.

By taking a closer look at Figure 12a and b, the short-fiber deposition pattern (Figure 12a) is likely the result of shifting the long-fiber deposition patter (Figure 12b) along the x-axis to the right (and vice versa). The shift along the x-axis implies the flow rate change, which is relevant to the impaction parameter. Thus, our data proves once again that carbon fibers depositing in the nasal airway is mainly due to impaction, and that short fibers could have the same deposition fraction as long fibers

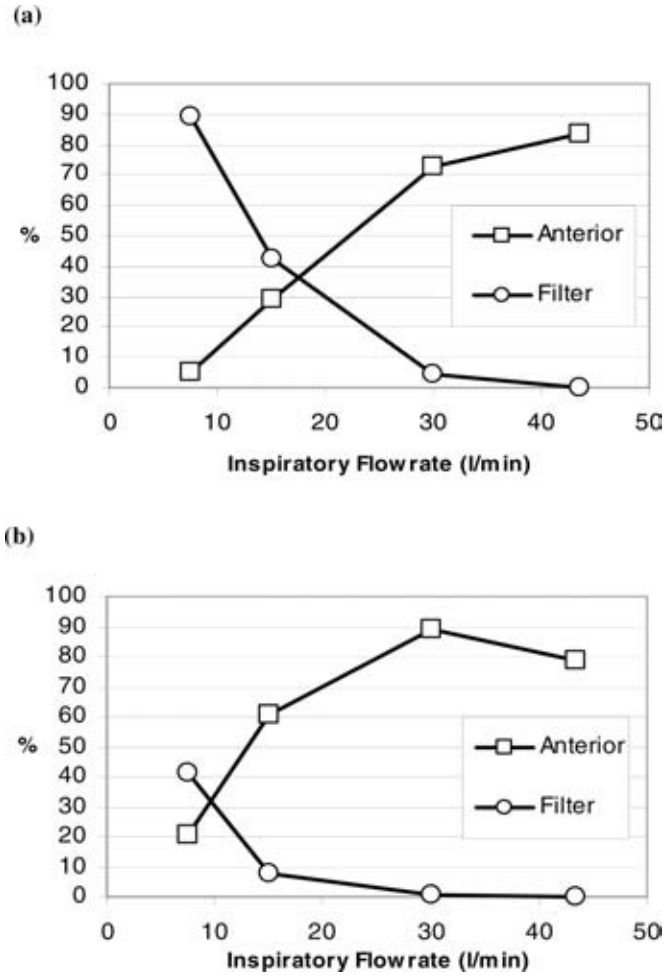

FIG. 12. Comparison of fiber deposition fraction in the anterior region and filter for (a) short fibers with fiber length 10–20 μm, and (b) long fibers with fiber length >200 μm.

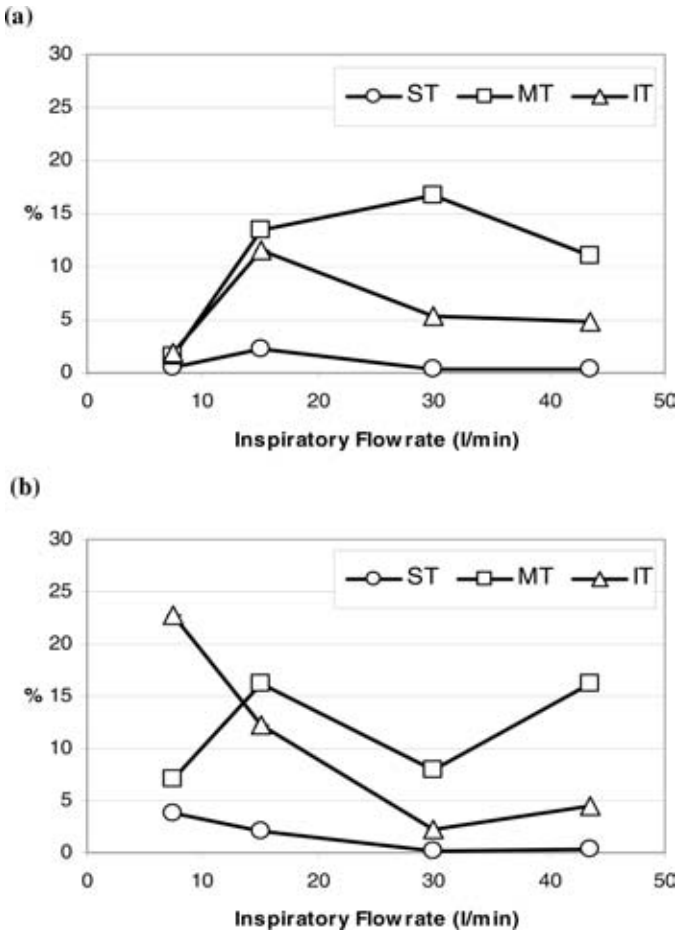

FIG. 13. Fiber deposition fraction in the turbinate region (a) short fibers with fiber length 10–20 μm, and (b) long fibers with fiber length >200 μm. (ST, MT, and IT: superior, middle, and inferior turbinate, respectively.)

in a specific nasal airway region or subregion, as long as the impaction parameter for both fibers are in the same range.

Fiber Deposition in the Turbinate Region

The turbinate region is a unique part in the human nasal airway. Its uniqueness is mainly due to its complicated structure and slot-like airway. Therefore, it is worth investigating the details of the deposition information in this region.

Subramaniam et al. (1998) used a computational fluid dynamics model to simulate the airflow profile in a human nasal airway (the same MRI scans as used in this research) and provided quantitative data of airspeed distribution in the nasal airway. In their research, Subramaniam et al. indicated that, the airflow in the IT and MT is basically flowing parallel with the nasal floor and the ST has the lowest airspeed and volumetric flow. These simulation results could greatly facilitate the understanding of the fiber deposition in the turbinate region. Figure 13 shows the fiber deposition fraction in the turbinate region for short fibers (Figure 13a) and long fibers (Figure 13b). As can be seen, overall, very few fibers were deposited in the turbinate region. The deposition fractions in each turbinate subregion were all below 25%. The deposition fraction of fibers in the ST has the lowest deposition fraction compared to that of the MT and IT; and the MT is basically greater than that of the IT except for long fibers in the low inspiratory flow rate (7.5 l/min). In order to explain these experimental results, the simulation results from Subramaniam et al. (1998) mentioned above could be applied here. First, because the airflow passing through the MT and IT is parallel with the nasal floor (also with the walls), it is hard for fibers to deposit on the floor and walls of the MT and IT by impaction. Thus, the fiber deposition fraction in these subregions was relatively low. Second, the lowest fiber deposition fraction in the ST is the result of only a little airflow passing through this area (in other words, only a few fibers were delivered into this area). Finally, it was shown that the fiber deposition in the MT was larger than that in the IT for inspiratory flow rates ranging from 15 l/min to 43.5 l/min. This might be due to the turbinate structure in the front turbinate region as indicated by Zwartz and Guilmette (2001). In their research, Zwartz and Guilmette found that the nasal airway has its MT suddenly protrude into the main airway. Therefore, fibers had more of a chance to impact on the front section of the MT where it faces the airflow. More deposition was thereby made on the MT in the front turbinate subregion as shown in Figures 5–8.

Comparison of Deposition Efficiency for Fiber and Spherical Particles

As has been mentioned in previous sections, some nasal airway deposition studies have been carried out with spherical particles, and used the nasal airway replicas with the same MRI

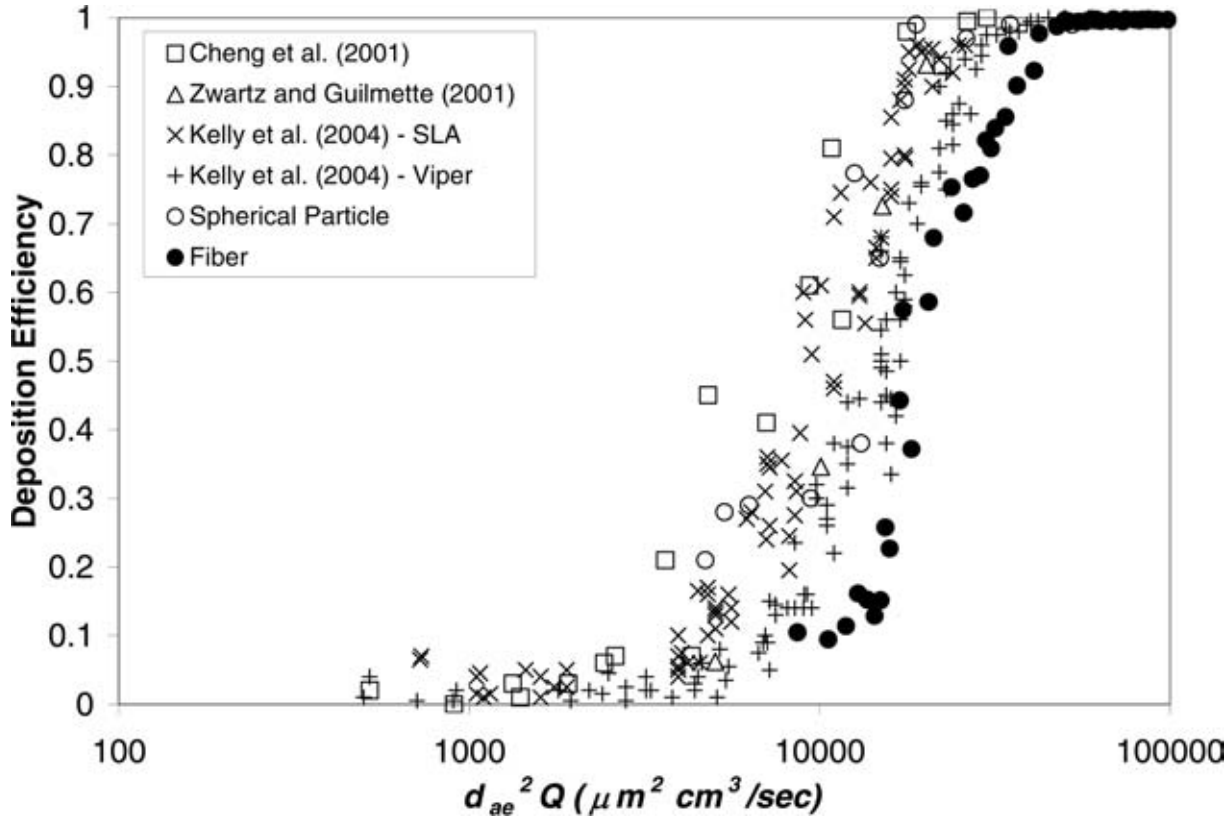

FIG. 14. Comparison of deposition efficiencies between fibers and spherical particles.

scans as used in this research (Cheng et al. 2001b; Zwartz and Guilmette 2001; Kelly 2004). In those studies, deposition efficiencies were obtained based on the nasal airway as an entire unit. Figure 14 compares the nasal airway deposition efficiency between spherical particles and carbon fibers. As can be seen, the trends of the deposition efficiencies are similar for both spherical particles and fibers. The deposition efficiency is a function of impaction parameter ($d_{ae}{}^2 Q$), and the deposition efficiency increases as the impaction parameter $d_{ae}{}^2 Q$ increases. The deposition efficiencies reach almost 100% as $d_{ae}{}^2 Q > 50000$ for both spherical particles and fibers. However, for $d_{ae}{}^2 Q < 50000$, the deposition efficiency of fibers is significantly lower than that of spherical particles. In order to verify this result and to investigate whether it is the experimental method used in this research that caused the difference, several more deposition experiments were conducted in present research using two sizes (6 μm and 10 μm) dyed polymer spherical particles (Fluorescent Microspheres, Duke Scientific Co., Palo Alto, California). Deposition experiments were conducted using the similar experimental method as for the fiber study. The only difference is that the deposition information was acquired by measuring the florescence intensity of the washed-out solution for each nasal airway region. The retest showed that (1) the new deposition efficiencies of the spherical particles obtained from present research agree well with those data acquired from other studies (see Figure 14), and (2) it is apparent that the deposition efficiency of fibers is indeed lower than that of spherical particles. This result implies that fibers inhaled by nose can pass through the nasal airway relatively easier than spherical particles. Therefore, fibers may have more of a chance, compared with spherical particles, to enter the lower respiratory tract—the deep lung.

Although some theoretical calculations (Asgharian 1988; Chen and Yu 1991; Asgharian et al. 1997) and experimental observation (Myojo 1987) have shown that fibers tend to align themselves to the flow direction, which might provide an explanation for the difference of the deposition efficiencies, further research is still needed to investigate whether this phenomena is also true in the tortuous flow field, such as the airflow in the human nasal airway.

CONCLUSION

In this research, experiments were conducted to investigate the effects of fiber length on the deposition pattern in the human nasal airway. MMVF-like carbon fibers with uniform diameter were adopted as the test material. A human nasal airway replica with realistic and well-defined airway geometry was used. This nasal airway was made from acrylic plates and consisted of nasal airway structures from nostril to nasopharynx. Deposition studies were conducted by delivering aerosolized carbon fiber into the nasal airway at constant inspiratory flow rates from 7.5 to 43.5 l/min. The deposition results showed that impaction is the dominant deposition mechanism. Fibers with high inertia were deposited on the anterior region of the nasal airway (vestibule); however, most fibers with low inertia were found to pass through the entire nasal airway and enter the lung. Comparing the deposition efficiency of fibers and spherical particles in the nasal airway showed that the deposition efficiency of fiber is generally lower than that of spherical particles. Further research might be needed to investigate the behavior of fiber in a complex flow field to explain the difference found. The deposition information acquired from this research could be applied in predicting fiber nasal deposition, and assessing the exposure dosimetry for other fibers, including asbestos and new MMVFs.

REFERENCES

Asgharian, B. (1988). Theoretical Deposition of Fibrous Particles in the Respiratory System of Human and Rats. Doctoral dissertation, University of New York at Buffalo, Buffalo.

Asgharian, B., Zhang, L., and Fang, C. P. (1997). Theoretical Calculations of the Collection Efficiency of Spherical Particle and Fibers in an Impactor, *J. Aerosol Sci.* 28:277–287.

Bernstein, D. M. Riego Sintes, J. M., Ersboell, B. K., and Kunert, J. (2001). Biopersistence of Synthetic Mineral Fibers as a Predictor of Chronic Intraperitoneal Injection Tumor Reponse in Rats, *Inhal. Toxicol.* 13:851–875.

Chen, Y. K., and Yu, C. P. (1991). Sedimentation of Fibers from Laminar Flows in a Horizontal Circular Duct, *Aerosol Sci. Technol*. 14:343–347.

Chen, B. T., Yeh, H. C., and Hobbs, C. H. (1993). Size Classification of Carbon Fiber Aerosols, *Aerosol Sci. Technol*. 19:109–120.

Cheng, Y. S., Powell, Q. H., Smith, S. M., and Johnson, N. F. (1995). Silicon Carbide Whiskers: Characterization and Aerodynamic Behavior, *Am. Ind. Hyg. Assoc. J*. 56:970–978.

Cheng, Y. S., Zhou, Y., and Chen, B. T. (1999). Particle Deposition in a Cast of Human Oral Airways, *Aerosol Sci. Technol*. 31:286–300.

Cheng, Y. S., Fu, C. S., Yazzie, D., and Zhou, Y. (2001a). Respiratory Deposition Patterns of Salbutamol pMDI with CFC and HFA-134a Formulations in a Human Airway Replica, *J. Aerosol Med.* 14(2):255–266.

Cheng, Y. S., Holmes, T. D., Gao, J., Guilmette, R. A., Li, S., Surakitbanharn, Y., and Rowlings, C. (2001b). Characterization of Nasal Spray Pumps and Deposition Pattern in a Replica of Human Nasal Airway, *J. Aerosol Med.* 14(2):267–280.

Guilmette, R. A., and Gagliano, T. J. (1994). Construction of a Model of Human Nasal Airways Using In Vivo Orphological Data, *Ann. Occup. Hyg*. 38:69–75.

Guilmette, R. A., Cheng, Y. S., Yeh, H. C., and Swift, D. L. (1994). Deposition of 0.005-12 μm Monodisperse Particles in a Computer-Milled MRI-Based Nasal Airway Replica, *Inhal. Toxicol.* 6(Suppl. 1):395–399.

Happel, J., and Brenner, H. (1973). Low Reynolds Number Hydrodynamics. Noordhoff, Leyden, p. 207.

Hesterberg, T. W., and Hart, G. A. (2001). Synthetic Vitreous Fibers: A Review of Toxicology Research and Its Impact on Hazard Classification, *Crit. Rev. Toxicol.* 31:1–53.

Hill, I. M., Beswick, P. H., and Donaldson, K. (1995). Differential Release of Superoxide Anions by Macrophages Treated with Long and Short Fibre Amosite Asbestos is a Consequence of Differential Affinity for Opsonin, *Occup. Environ. Med.* 52:92–95.

IARC. (1987). IARC Monographs on the Evaluation of Carcinogenic Risks to Humans, Supplement 7: Overall Evaluations of Carcinogenicity an Updating of IARC Monographs Vol. 1-42. Lyon, IARC Press, p. 106.

IARC. (2002). IARC Monographs on the Evaluation of Carcinogenic Risks to Humans, Vol. 81, Man-made Vitreous Fibers, Lyon, IARC Press.

Kamstrup, O., Ellehauge, A., Collier, C. G., and Davis, J. M. G. (2002). Carcinogenicity Studies after Intraperitoneal Injection of Two Types of Stone Wool Fibres in Rats, *Ann. Occup. Hyg.* 46(2):135–142.

Kelly, J. T., Asgharian, B., Kimbell, J., and Wong, B. A. (2004). Particle Deposition in Human Nasal Airway Replicas Manufactured by Different Methods. Part I: Inertial Regime Particles, *Aerosol Sci. Technol.* 38:1036–1071.

Lippman, M. (1990). Effects of Fiber Characteristics on Lung Deposition, Retention, and Disease, *Environ. Health Perspect.* 88:311–317.

Miller, B. G., Searl, A., Davis, M. G., Donaldson, K., Cullen, R. T., Bolton, R. E., Buchanan, D., and Soutar, C. A. (1999). Influence of Fibre Length, Dissolution and Biopersistence on the Production of Mesothelioma in the Rat Peritoneal Cavity, *Ann. Occup. Hyg.* 43(3):155–166.

Myojo, T. (1987). Deposition of Fibrous Aerosol in Model Bifurcating Tubes, *J. Aerosol Sci.* 18:337–347.

Myojo, T. (1990). The Effect of Length and Diameter on the Deposition of Fibrous Aerosol in a Model Lung Bifurcation, *J. Aerosol Sci.* 21:651–659.

NIOSH. (1994). Asbestos and Other Fibers by PCM. NIOSH Manual of Analytical Method.

Selikoff, I. J., and Lee, D. H. (1978). *Asbestos and Disease*. Academic Press, New York.

Stöber, W., Flachsbart, H., and Hochrainer, D. (1970). The Aerodynamic Diameter of Latex Aggregates and Asbestos Fibres, *Staub-Reinhalt Luft*, 30:1–12.

Stöber, W. (1972). Dynamic Shape Factors of Nonspherical Aerosol Particles. In *Assessment of Airborne Particles*, T. Mercer et al., eds., Charles C. Thomas Publisher, Springfield, IL, pp. 249–289.

Subramaniam, R. P., Richardson, R. B., Morgan, K. T., Kimbell, J. S., and Guilmette, R. A. (1998). Computational Fluid Dynamics Simulations of Inspiratory Airflow in the Human Nose and Nasopharynx, *Inhal. Toxicol*. 10:91–120.

Sussman, R. G., Cohen, B. S., and Lippmann, M. (1991). Asbestos Fiber Deposition in Human Tracheobronchial Cast. I. Experimental, *Inhal. Toxicol.* 3:145–160.

Swift, D. L. (1991). Inspiratory Inertial Deposition of Aerosols in Human Nasal Airway Replicate Casts: Implication for the Proposed NCRP Lung Model, *Rad. Prot. Dosimetry*. 38(1/3):29–34.

Timbrell, V. (1982). Deposition and Retention of Fibers in Human Lung, *Ann. Occup. Hyg.* 26:347–369.

WHO. (2000). Man-made Vitreous Fibers. In *Air Quality Guidelines*, Second Ed., Chapter 8.2, World Health Organization.

Zhou, Y., and Cheng, Y. C. (2005). Particle Deposition in a Cast of Human Tracheobronchial Airways, *Aerosol Sci. Technol.* 39:49.

Zwartz, G. J., and Guilmette, R. A. (2001). Effect of Flow Rate on Particle Deposition in a Replica of a Human Nasal Airway, *Inhal. Toxicol*. 13:109–127.